Multi-modality optical neural imaging using coherence control of VCSELs

Elizabeth A. Munro,[1] Hart Levy,[1,2] Dene Ringuette,[1] Thomas D. O'Sullivan,[3] and Ofer Levi[1,2,*]

[1]*Institute of Biomaterials and Biomedical Engineering, University of Toronto, 164 College Street, Toronto, Ontario, M5S 3G9, Canada*

[2]*The Edward S. Rogers Sr. Department of Electrical and Computer Engineering, University of Toronto, 10 King's College Road, Toronto, Ontario, M5S 3G4, Canada*

[3]*Beckman Laser Institute and Medical Clinic, 1002 Health Sciences Rd, Irvine, CA 92612, USA*

**ofer.levi@utoronto.ca*

Abstract: Neural optical imaging can evaluate cortical hemodynamic fluctuations which reflect neural activity and disease state. We evaluate the use of vertical-cavity surface-emitting lasers (VCSELs) as illumination source for simultaneous imaging of blood flow and tissue oxygenation dynamics *ex vivo* and *in vivo* and demonstrate optical imaging of blood flow changes and oxygenation changes in response to induced ischemia. Using VCSELs we show a rapid switching from a single-mode to a special multi-mode rapid current sweep operation and noise values reduced to within a factor of 40% compared to non-coherent LED illumination. These VCSELs are promising for long-term portable continuous monitoring of brain dynamics in freely moving animals.

OCIS codes: (170.0110) Imaging systems; (170.3880) Medical and biological imaging; (140.2020) Laser diodes; (170.6480) Spectroscopy, speckle.

References and links

1. D. A. Boas and A. K. Dunn, "Laser speckle contrast imaging in biomedical optics," J. Biomed. Opt. **15**(1), 011109 (2010).
2. J. D. Briers, "Laser Doppler, speckle and related techniques for blood perfusion mapping and imaging," Physiol. Meas. **22**(4), R35–R66 (2001).
3. A. Ponticorvo and A. K. Dunn, "How to build a Laser Speckle Contrast Imaging (LSCI) system to monitor blood flow," J. Vis. Exp. **45**(45), (2010), http://www.jove.com/details.stp?id=2004.
4. O. Yang, D. Cuccia, and B. Choi, "Real-time blood flow visualization using the graphics processing unit," J. Biomed. Opt. **16**(1), 016009–016014 (2011).
5. J. C. Ramirez-San-Juan, R. Ramos-García, I. Guizar-Iturbide, G. Martínez-Niconoff, and B. Choi, "Impact of velocity distribution assumption on simplified laser speckle imaging equation," Opt. Express **16**(5), 3197–3203 (2008).
6. A. B. Parthasarathy, S. M. S. Kazmi, and A. K. Dunn, "Quantitative imaging of ischemic stroke through thinned skull in mice with Multi Exposure Speckle Imaging," Biomed. Opt. Express **1**(1), 246–259 (2010).
7. J. C. Ramírez-San-Juan, Y. C. Huang, N. Salazar-Hermenegildo, R. Ramos-García, J. Muñoz-Lopez, and B. Choi, "Integration of image exposure time into a modified laser speckle imaging method," Phys. Med. Biol. **55**(22), 6857–6866 (2010).
8. C. Zhou, S. A. Eucker, T. Durduran, G. Yu, J. Ralston, S. H. Friess, R. N. Ichord, S. S. Margulies, and A. G. Yodh, "Diffuse optical monitoring of hemodynamic changes in piglet brain with closed head injury," J. Biomed. Opt. **14**(3), 034015 (2009).
9. T. Durduran, C. Zhou, B. L. Edlow, G. Q. Yu, R. Choe, M. N. Kim, B. L. Cucchiara, M. E. Putt, Q. Shah, S. E. Kasner, J. H. Greenberg, A. G. Yodh, and J. A. Detre, "Transcranial optical monitoring of cerebrovascular hemodynamics in acute stroke patients," Opt. Express **17**(5), 3884–3902 (2009).
10. M. J. Rossow, W. W. Mantulin, and E. Gratton, "Scanning laser image correlation for measurement of flow," J. Biomed. Opt. **15**(2), 026003 (2010).
11. O. B. Thompson and M. K. Andrews, "Tissue perfusion measurements: multiple-exposure laser speckle analysis generates laser Doppler-like spectra," J. Biomed. Opt. **15**(2), 027015 (2010).
12. A. Grinvald, E. Lieke, R. D. Frostig, C. D. Gilbert, and T. N. Wiesel, "Functional architecture of cortex revealed by optical imaging of intrinsic signals," Nature **324**(6095), 361–364 (1986).

#142244 - $15.00 USD Received 4 Feb 2011; revised 10 May 2011; accepted 16 May 2011; published 18 May 2011

13. V. A. Kalatsky and M. P. Stryker, "New paradigm for optical imaging: temporally encoded maps of intrinsic signal," Neuron **38**(4), 529–545 (2003).
14. A. Grinvald, R. Siegel, E. Bartfeld, and R. D. Frostig, "High resolution optical imaging of functional architecture in the awake primate," Soc. Neurosci. Abstracts **17**, 1016 (1991).
15. R. D. Frostig, E. E. Lieke, D. Y. Ts'o, and A. Grinvald, "Cortical functional architecture and local coupling between neuronal activity and the microcirculation revealed by *in vivo* high-resolution optical imaging of intrinsic signals," Proc. Natl. Acad. Sci. U.S.A. **87**(16), 6082–6086 (1990).
16. C. H. Chen-Bee, T. Agoncillo, Y. Xiong, and R. D. Frostig, "The triphasic intrinsic signal: implications for functional imaging," J. Neurosci. **27**(17), 4572–4586 (2007).
17. E. M. Hillman, "Optical brain imaging *in vivo*: techniques and applications from animal to man," J. Biomed. Opt. **12**(5), 051402 (2007).
18. E. Gratton, V. Toronov, U. Wolf, and M. Wolf, "Detection of brain activity by near-infrared light," in *Biomedical Optical Imaging*, J. G. Fujimoto and D. Farkas, eds. (Oxford University Press, New York, 2009), p. 356.
19. M. Wolf, M. Ferrari, and V. Quaresima, "Progress of near-infrared spectroscopy and topography for brain and muscle clinical applications," J. Biomed. Opt. **12**(6), 062104 (2007).
20. T. Hamaoka, K. K. McCully, V. Quaresima, K. Yamamoto, and B. Chance, "Near-infrared spectroscopy/imaging for monitoring muscle oxygenation and oxidative metabolism in healthy and diseased humans," J. Biomed. Opt. **12**(6), 062105 (2007).
21. H. Watanabe, F. Homae, T. Nakano, and G. Taga, "Functional activation in diverse regions of the developing brain of human infants," Neuroimage **43**(2), 346–357 (2008).
22. M. B. Bouchard, B. R. Chen, S. A. Burgess, and E. M. Hillman, "Ultra-fast multispectral optical imaging of cortical oxygenation, blood flow, and intracellular calcium dynamics," Opt. Express **17**(18), 15670–15678 (2009).
23. P. B. Jones, H. K. Shin, D. A. Boas, B. T. Hyman, M. A. Moskowitz, C. Ayata, and A. K. Dunn, "Simultaneous multispectral reflectance imaging and laser speckle flowmetry of cerebral blood flow and oxygen metabolism in focal cerebral ischemia," J. Biomed. Opt. **13**(4), 044007 (2008).
24. A. K. Dunn, A. Devor, H. Bolay, M. L. Andermann, M. A. Moskowitz, A. M. Dale, and D. A. Boas, "Simultaneous imaging of total cerebral hemoglobin concentration, oxygenation, and blood flow during functional activation," Opt. Lett. **28**(1), 28–30 (2003).
25. Z. Luo, Z. Yuan, Y. Pan, and C. Du, "Simultaneous imaging of cortical hemodynamics and blood oxygenation change during cerebral ischemia using dual-wavelength laser speckle contrast imaging," Opt. Lett. **34**(9), 1480–1482 (2009).
26. Y. B. Sirotin, E. M. C. Hillman, C. Bordier, and A. Das, "Spatiotemporal precision and hemodynamic mechanism of optical point spreads in alert primates," Proc. Natl. Acad. Sci. U.S.A. **106**(43), 18390–18395 (2009).
27. T. O'Sullivan, E. A. Munro, N. Parashurama, C. Conca, S. S. Gambhir, J. S. Harris, and O. Levi, "Implantable semiconductor biosensor for continuous *in vivo* sensing of far-red fluorescent molecules," Opt. Express **18**(12), 12513–12525 (2010).
28. R. Michalzik and K. J. Ebeling, "Operating principles of VCSELs," in *Vertical-Cavity Surface-Emitting Laser Devices*, H. Li and K. Iga, eds. (Springer-Verlag, Berlin, 2003), pp. 53–98.
29. T. T. Lee, P. G. Lim, J. S. Harris, Jr., K. V. Shenoy, and S. J. Smith, "Low-frequency noise characterization of near-IR VCSELs for functional brain imaging," Proc. SPIE **6852**, 68422T, 68422T-8 (2008).
30. A. J. Foust, J. L. Schei, M. J. Rojas, and D. M. Rector, "In vitro and *in vivo* noise analysis for optical neural recording," J. Biomed. Opt. **13**(4), 044038 (2008).
31. B. E. A. Saleh and M. C. Teich, *Fundamentals of Photonics*, 2nd ed., Wiley Series in Pure and Applied Optics (Wiley, Hoboken, NJ, 2007).
32. J. W. Goodman, "Some fundamental properties of speckle," J. Opt. Soc. Am. **66**(11), 1145–1150 (1976).
33. G. Craggs, G. Verschaffelt, S. K. Mandre, H. Thienpont, and I. Fischer, "Thermally controlled onset of spatially incoherent emission in a broad-area vertical-cavity surface-emitting laser," IEEE J. Sel. Top. Quantum Electron. **15**(3), 555–562 (2009).
34. A. B. Parthasarathy, W. J. Tom, A. Gopal, X. J. Zhang, and A. K. Dunn, "Robust flow measurement with multi-exposure speckle imaging," Opt. Express **16**(3), 1975–1989 (2008).
35. P. Zakharov, A. C. Völker, M. T. Wyss, F. Haiss, N. Calcinaghi, C. Zunzunegui, A. Buck, F. Scheffold, and B. Weber, "Dynamic laser speckle imaging of cerebral blood flow," Opt. Express **17**(16), 13904–13917 (2009).
36. D. D. Duncan and S. J. Kirkpatrick, "Can laser speckle flowmetry be made a quantitative tool?" J. Opt. Soc. Am. A **25**(8), 2088–2094 (2008).

1. Introduction

Optical imaging techniques for biomedical applications show significant advantages over other imaging modalities like fMRI, PET, and CT due to their flexible system design, low cost, small size and potential for widespread applications. Noninvasive optical imaging techniques that provide anatomical and functional information on the brain are attractive

#142244 - $15.00 USD Received 4 Feb 2011; revised 10 May 2011; accepted 16 May 2011; published 18 May 2011

candidates for *in vivo* preclinical studies and patient care. Two optical imaging techniques in particular offer high temporal and spatial resolution and have great potential for use in portable optical brain imaging studies. These two techniques are Laser Speckle Contrast Imaging (LSCI) and Intrinsic Signal Optical Imaging (ISOI).

LSCI is a minimally invasive method used to image blood flow *in vivo* to obtain relative quantification of blood flow rates (i.e. speed of moving particles in a vessel) with high spatial and temporal resolution utilizing the interference effects of a coherent source [1–3]. Scattering of coherent laser light within tissue produces a characteristic random interference pattern known as speckle. Non-moving scattering particles in the media produce a stable speckle pattern, whereas movement of scattering particles causes phase shifts in the scattered light and temporal changes in the speckle pattern. In LSCI, time-integrated speckle pattern can be used to estimate blood flow in a tissue. The spatial speckle contrast ratio (CR) is a measure of speckle spatial statistics, which can be related to coherence time, a quantity inversely proportional to particle velocity. The spatial CR is defined as the ratio of the spatial standard deviation σ to the mean intensity $\langle I \rangle$ by

$$CR_{Speckle} = \sigma / \langle I \rangle \tag{1}$$

CR values can be used to evaluate flow rates. As reviewed in detail in [1], the electric field autocorrelation function $g_1(\tau)$, is assumed to have an exponential decay form with a characteristic time τ_c. The correlation time τ_c represents a characteristic decay time of the backscattered speckle and is used to measure the blood flow in LSCI. τ_c is assumed to be inversely proportional to the blood flow velocity. Using a fixed exposure time during image acquisition, qualitative relative flow values in vasculature can be mapped by calculating values of τ_c from CR values [4,5]. However, more quantitative and accurate relative flow values can be obtained using sequentially varied camera exposure times and adequate flow calibration [6,7]. Diffuse correlation spectroscopy (DCS) is an alternate method of evaluating blood flow in the brain [8] and has been successfully applied in evaluation of cerebral blood flow in stroke patients [9]. However, this technique requires the use of fiber-coupled laser diodes along with photon-counting fast avalanche photodiode detectors or photomultiplier tubes to evaluate the light intensity auto-correlation, resulting in lower spatial resolution and a complex optical measurement system. The Scanning Laser Image Correlation (SLIC) technique [10] makes use of line scan correlations across vessels to obtain a slope representing flow velocities. However, the use of laser scans in SLIC requires substantially more time to map an entire cranial region, as well as vessel path mapping and further data processing to obtain accurate values, decreasing the simplicity and speed of this technique. Laser Doppler is another flowmetry technique commonly used clinically. Recent studies show multi exposure LSCI techniques give blood flow information similar to laser Doppler flow measurements [11].

ISOI is a functional brain imaging technique which has been used for over two decades to obtain maps of cortical activation [12] and is widely used in neuroscience studies and evaluating brain plasticity [13–16]. It provides high spatial resolution maps (~10 μm) of stimulus-evoked hemodynamic-related signals as an indirect means to map evoked neuronal activity. This technique typically uses an external light source to illuminate the cortex and a wide area image sensor imager such as a CCD camera to record changes in light reflectance. Optical reflectance changes in intact tissue are caused by fluctuations of blood volume, blood flow and intrinsic chromophore levels: primarily oxygenated (HbO_2) and deoxygenated hemoglobin (HbR). These changes are associated with changes in oxygen delivery and consumption in the brain and in blood vessel diameter [17,18]. They occur during increased metabolic activity, which is a direct correlate of neuronal activation. While intensity changes in injected voltage sensitive dyes and Ca^+ sensitive dyes induced by neuronal activity are often brighter and more easily resolved, ISOI provides a high resolution, less invasive

#142244 - $15.00 USD Received 4 Feb 2011; revised 10 May 2011; accepted 16 May 2011; published 18 May 2011

approach to brain imaging. In recent years, multiple illumination wavelengths enabled spectral analysis of ISOI values and creating maps of HbO_2 and HbR concentrations [17]. In clinical studies, the related technique of Near Infrared Spectroscopy (NIRS) is often used to determine hemoglobin concentrations in human tissues [19,20]. Difficulties with this technique arise from the necessity of imaging through intact skull, producing low resolution and increased noise, though many applications in infants have proved effective [21].

Combining blood flow information from LSCI and oxygenation from ISOI can provide a better estimate of underlying neural activity and cortical dynamics. In recent years, there have been several research activities toward this goal [22–25]. Conventional ISOI setups employ a large size camera, lamp or LEDs as a light source, bulky imaging optics and require the subject to be immobile during image acquisition. Our goal is to create a portable miniaturized optical neural imaging system which can be implanted on top of the brain region of interest to allow for continuous imaging of neural activity while the subject is awake and freely behaving. In order to achieve a portable head-mounted continuous imaging technique to simultaneously observe blood flow and oxygenation changes in animal brains, there is a need to simplify the imaging system and combine light sources and cameras for LSCI and ISOI. It will offer means for studying the underlying neuronal activity in un-anesthetized animals, and help meet the increased demand for long-term *in vivo* brain imaging created by the rapid appearance of new stem cell therapies and improved drugs for brain diseases. Furthermore, a continuous imaging modality in a clinical setting is a key component in creating personalized treatment plans based on up-to-the-minute disease progression and drug efficacy monitoring.

Tissue reflectance-based imaging techniques such as ISOI require low noise illumination sources and typically non-coherent light sources such as LEDs have been used [16,22,26], avoiding the complications associated with laser speckle. However, the use of semiconductor lasers, if properly implemented, introduces several advantages over LEDs including increased brightness, facilitated focusing capabilities and smaller device footprint. In addition to the inherent benefits they offer to ISOI, coherent laser diodes can be used to simultaneously provide additional information about cerebral blood flow using LSCI [23,25] or Doppler techniques, as well as a high-brightness source for multi-modality fluorescence imaging of the brain tissue. Modules of such a system, including low-noise detectors and high brightness vertical-cavity surface-emitting lasers (VCSELs) were recently fabricated and demonstrated for continuous monitoring of fluorescence from tumors in live animals [27].

In this work we evaluate VCSELs as light sources for optical neural imaging *ex vivo* and *in vivo*. VCSELs have emerged as a high-brightness, low cost, power efficient solution to many applications including optical communication and optical interconnects. In particular, oxide-confined VCSELs have emerged as a viable commercial solution with wavelengths as low as 670 nm, power levels in excess of 1 mW, circular beam shape, low noise, over a GHz modulation bandwidth and good control of the mode shape and optical beam properties as reviewed by Michalzik *et al.* [28]. These VCSELs have been shown to be stable and have low values of relative intensity noise (RIN) [29]. Power efficiency, small size and low operating currents (~few mA) minimize the required operating power and heat dissipation requirements, making VCSELs attractive light sources for portable imaging applications.

Previous studies have shown that time-varying speckle patterns in reflected light from neural tissue due to the coherence of laser diodes can lead to a lower signal-to-noise ratio (SNR) in both *in vitro* and *in vivo* neural studies and mitigate the benefits they may have over LEDs [30]. Our initial ISOI studies, imaging the mouse visual cortex *in vivo* and using LEDs and VCSELs as light sources have shown a similar trend. Further analysis has shown that the speckle pattern on the brain tissue due to a VCSEL's coherence properties is the main challenge in producing low-noise illumination required for evaluating tissue oxygenation.

As shown below, we compared the measured noise values in reflection from a stationary opal glass, *ex vivo* from a brain slice of a mouse brain, and *in vivo* illuminating a rat brain using VCSELs at 670 nm and demonstrate a novel low-noise VCSEL operating scheme,

#142244 - $15.00 USD Received 4 Feb 2011; revised 10 May 2011; accepted 16 May 2011; published 18 May 2011

suitable for ISOI brain imaging. The VCSEL coherence can be used to estimate blood flow in the tissue simultaneously using the LSCI technique, all in a miniature package and suitable for portable continuous imaging applications. A common metric in measuring coherence effects is evaluating a coherence length. The coherence length l_c of a laser source is associated with the spectral linewidth of the laser according to [31]:

$$l_c = \frac{2\ln 2}{\pi}\frac{\lambda^2}{\Delta\lambda_{1/2}} \tag{2}$$

Where λ is the laser operating wavelength and $\Delta\lambda_{1/2}$ is the FWHM spectral width. The coherence length l_c can be reduced by operating the laser in a multi-mode operating regime, where multiple transverse modes are supported and the spectral bandwidth is increased. This change in l_c leads to a reduction in the speckle contrast magnitude. When a surface is illuminated by light with separate wavelength components to create M uncorrelated speckle patterns, they will add on an irradiance basis to reduce the speckle contrast magnitude by $1/\sqrt{M}$ [32]. We hypothesize that speckle magnitude can be further reduced by cycling between different multi-mode states, while keeping a longer integration time in a detector or a CCD camera. This novel technique allows for temporal blending of spatially varying speckle interference patterns (as operating current changes induce spatial changes in transverse mode patterns) as well as polarization states while imaging brain tissues.

The paper is organized as follows: in Section 2 we discuss the materials and methods used in this study; in Section 3 we detail the noise values obtained in the various VCSEL operating schemes, compare these values to noise values from an LED and demonstrate optical imaging of the brain during an ischemia event; finally, in Section 4 we discuss the implications of these findings to portable optical imaging systems.

2. Materials and methods

2.1 Imaging system

A schematic of the experimental setup is shown in Fig. 1 (a). A CCD camera is used for imaging the inspected surface (i.e. opal glass, mouse brain tissue, live rat brain), while LED (625 nm) and VCSEL (670 nm) light sources are used for illumination in various operating modes. Both opal glass and brain tissue images were processed to retrieve temporal noise and spatial contrast data values, discussed in section 3.3. The backscattered light is collected using a 1:1 magnification with two identical lenses (Nikon, F = 50mm, F/1.4) into the CCD camera for opal glass and live rat brain imaging studies. The camera was mounted on a vertical translation stage, allowing adjustment of the focal plane height. The imaged field of view was 7.6 x 7.6 mm. Slice imaging for mouse brain tissue slices was conducted through a microscope (BX51, Olympus, Japan) with low magnification objective (XL Fluor 4x/340, x4 magnification, NA 0.28). A cross section schematic of a VCSEL is shown in Fig. 1 (b).

LED and VCSEL illumination are alternated using a fast switch (Model 7001, Keithley, Cleveland, OH). The switch settling time is less than 200 μs, with less than 13 μs jitter, and by making use of a switch-ready signal to initiate frame capture, it is ensured that the camera frame rate is the only relevant factor in switching speed. The CCD camera (Retiga 4000R, QImaging, Surrey, BC) was triggered to collect 1024x1024 pixel, 12 bit images at 8 Hz, in synchronization with the source alternation. The rapid switching scheme allowed source alternation less than 200 μs after each trigger, with timing jitter below 13 μs. In total, alternating frames of each source were obtained at 4 frames per second. Following image sequence recording, the images were processed to retrieve temporal noise values and spatial statistics of speckle patterns. The resulting speckle contrast values can also be used to calculate speckle decorrelation times and relative flow rates [6].

#142244 - $15.00 USD Received 4 Feb 2011; revised 10 May 2011; accepted 16 May 2011; published 18 May 2011

Control of the VCSEL with a low noise current source (Model 6221, Keithley, Cleveland, OH) allowed for excitation of several different laser operation schemes, each of which was compared directly to LED illumination:

- *Single mode* illumination (SM) was produced with the laser driven near threshold current (5-6 mA), generating a roughly Gaussian beam profile.
- *Multi mode* illumination (MM) was produced by driving the laser at peak output (14.5 mA), at which point the gain profile excites multiple transverse modes, producing a spotted torus-shaped beam.
- *Sweep mode* illumination (SW) was produced by applying a 10 kHz sinusoidal sweep of current of 7-14.5 mA, inducing a rapid averaging of the multiple modes and shifting power spectrum.

Opal diffusing glass (50 mm square, Edmund Optics, Barrington, NJ) was used for assessment of noise values and spatial statistics of speckle patterns from a known stationary imaging surface. These values can be used to discern how the speckle pattern itself varies between light sources and between the various VCSEL operating modes, while mitigating temporal effects, to isolate some of the noise sources present *in vivo*.

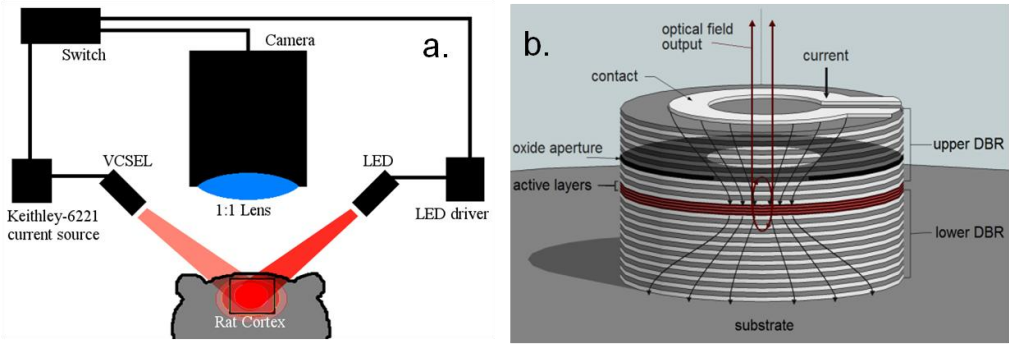

Fig. 1. Experimental setup. (a) CCD camera utilizes two identical camera lenses to maintain one-to-one magnification. The switch is trigger-linked to the camera to alternate the illumination source every frame between an LED and a VCSEL. (b) cross section schematic of a VCSEL, where the effect of oxide aperture to confine the current inside the cavity is illustrated.

2.2 Animal preparation for ex vivo mouse brain slices

All experimental procedures were approved by the Animal Care and Use Committee at the University of Toronto and the affiliated University Health Network hospitals. Mouse brain coronal slices (thickness ~400 μm) were prepared and immersed in artificial cerebrospinal fluid (ACSF) in a flow chamber during the noise evaluation studies. These slices typically included a hippocampus region as well as a parietal cortex region. The slices were stabilized in ACSF for over an hour prior to imaging studies. Slice movement during imaging was minimized by the design of the flow chamber and further immobilization was provided by the recording electrode tip. Stimulation of spreading depression during slice imaging was done by local injection of 3mMolar Potassium Chloride (KCl) via a cellular injection system (Picospritzer, Parker Hannifin Corp., Cleveland, OH). All coherence noise values were estimated from the cortical regions. *Ex vivo* brain slice images were taken at a focus depth of 100 μm below the slice surface, to ensure imaging from within the slice, resulting in a reduced sensitivity to slice movement from ACSF flow.

#142244 - $15.00 USD Received 4 Feb 2011; revised 10 May 2011; accepted 16 May 2011; published 18 May 2011

2.3 Animal preparation for in vivo rat brain

Sprague Dawley rats (mass 300-350 g) were anesthetized with 5% Isoflurane in oxygen (at 1 L/min flow rate) delivered through a nose cone. The percentage of Isoflurane was reduced to 2-3% saturation during brain imaging sessions, ensuring throughout that the animals had no response to toe pinch. Animal body temperature was maintained at 37°C using a feedback controlled thermal blanket (T/Pump, Gaymar Industries, Orchard Park, NY) during the studies. The animal head was fixed in a stereotaxic frame (Kopf Instruments, Tujunga, CA). A 3 mm section of the skull between the bregma and lambda ridges was removed by craniotomy to partially expose one hemisphere of the parietal cortex, while not exposing the midline artery. A petroleum jelly wall was built around the exposed cortex. The resulting compartment was filled with agarose gel and overlaid with a glass cover slip to create a flat imaging plane. All *in vivo* rat brain images were taken at a focus depth of 600 μm below the cortical surface, imaging in the neural area associated with sensory stimulation.

2.4 Image analysis

For temporal analysis in live rat brains, 1000 images were taken with each VCSEL illumination scheme (i.e. SM, MM, SW) and compared to 1000 corresponding LED images, for n = 7 rats. The exposure times were kept identical, while comparing illumination schemes, in a range of 5–30 msec. Over the 1000 image sequence, the standard deviation over mean intensity $\sigma/\langle I \rangle = (\sigma/\mu)$ ratio was calculated on a per pixel basis. For each rat, the mean representative pixel value was recorded, and the variation in values was used to ensure statistical anomalies associated with outliers were mitigated. A similar analysis was repeated in all cases on the opal glass with n = 5 trials, and with brain slices with n = 5 trials. For one rat, a further temporal analysis experiment was conducted on trial repeated data to investigate the performance enhancement capabilities of trial averaging *in vivo*. In this case, sets of 256 images were taken with each illumination source. Set trials were repeated 64 times, and then combined to create a single set of 256 supercells for each of SM, SW and LED illumination schemes. For each source, temporal (σ/μ) image maps were produced for both the single trial case and for the 64 trial average.

Spatial noise analysis was conducted on individual images in all illumination schemes. Within a single frame, (σ/μ) calculations were made over a moving 5x5 pixels region of interest (ROI), centered sequentially at each pixel of the image [1]. The resulting spatial contrast map was then averaged over 40 images to obtain a short time scale statistical average. Contrast values were then averaged over the cortical imaging region to obtain the average spatial noise value. For *ex vivo* slices, in all cases the raw images were binned in 4x4 pixels, in order to compensate for the 4x magnification and the resulting increase in speckle size [1].

2.5 Source characterization

Spectra for the VCSEL in SM, MM and SW were measured using an optical spectrum analyzer (OSA) (Model AQ6370B, Yokogawa North America, Newnan, GA) and measured spectral width Δλ values were used to estimate the coherence length, l_c using Eq. (2). A Michelson interferometer was then used to more directly quantify the coherence length, l_c for verification [31]. In order to investigate the effects of transverse mode averaging, far field images of the laser beam spot were taken using the CCD with lenses removed. Operating currents ranging from 5 mA to 19 mA were imaged, along with SW operation.

3. Results

3.1 VCSEL transverse mode analysis

The VCSEL structure confines the field within a very short laser cavity, between two stacks of distributed Bragg reflector (DBR) mirrors as shown in Fig. 1 (b). The short cavity length (~5-10 μm) supports only one longitudinal mode. However, either a transverse single mode or

#142244 - $15.00 USD Received 4 Feb 2011; revised 10 May 2011; accepted 16 May 2011; published 18 May 2011

multimode operation is possible, depending on the VCSEL structure design [28]. Figure 2 shows the far field transverse mode behavior of a 670 nm oxide-confined VCSEL. Figure 2 (a) shows the mode intensity pattern for individual current values. With current values near lasing threshold (~5-6 mA), a fundamental transverse mode shape is observed. While this fundamental mode (SM) can be difficult to achieve in VCSELs, such as the one used in this work with a large oxide-aperture (10-12 μm), locating the oxide aperture higher in the top DBR stack of the VCSEL cavity allows such mode shape, at the expense of a raised threshold current and lower peak power. With increasing current, an onset of higher azimuthal order, donut-shaped, transverse mode for high currents is initiated by fundamental mode spatial hole burning and thermally induced waveguiding effects [28]. Furthermore, by increasing current values above ~15 mA, a typical rollover of the output power characteristics in observed. Figure 2 (b) shows the current sweep operation scheme (SW) where rapid current sweep, causing a temporal mixing of the laser modes shown in (a), to be observed in each camera frame as a more uniform beam profile with reduced coherence. Importantly, the ability to obtain both SM and SW operations in the same VCSEL, with reasonable power output, is a key step in using it as an illumination source simultaneously for both LCSI and ISOI, using one camera and rapid switching of the illumination patterns.

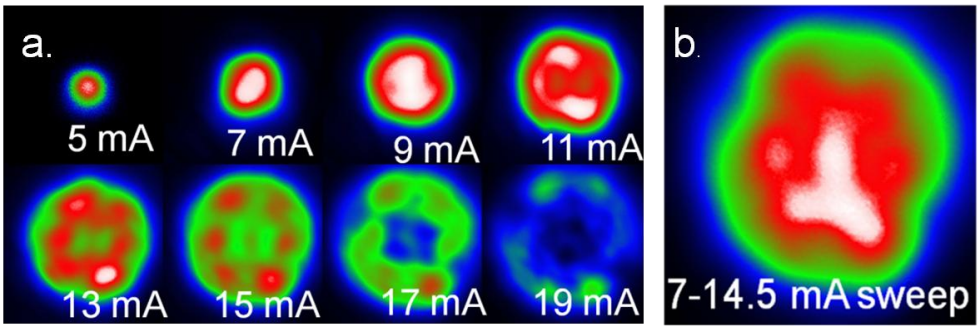

Fig. 2. Far field intensity mode patterns for a VCSEL. (a) mode profiles for various individual current values to the VCSEL. (b) SW operation (enlarged) integrates the transverse modes over a single camera exposure time, to produce a more uniform intensity pattern.

3.2 Coherence length evaluation

Figure 3 (a) shows the emission spectra for a 670 nm oxide-confined VCSEL at various VCSEL operation modes with currents of 5 mA (SM), 14.5 mA (MM) and a 7 to 14.5 mA sinusoidal current sweep (SW). A spectral broadening is observed in MM operation mode, most likely due to the limited resolution of the OSA in the presence of multiple close peaks. The thermal wavelength shift with increasing current is mainly governed by change of the average index of refraction of the cavity in a short VCSEL cavity. Spectral shift values of $\partial\lambda/\partial T \approx 0.06 nm/K$ can be used to estimate the internal temperature increase. In SW mode, an "effective" spectral broadening is observed due to temporal integration of all the spectral components of the modes within this current range in a rapid current sweep (~10 KHz). This spectral broadening also occurs when using camera exposure times in the order of a few msec, which are much longer as compared to the current sweep cycle. Utilizing Eq. (2), coherence lengths for each mode are estimated from the spectral $\Delta\lambda_{1/2}$ FWHM values. A Michelson interferometer can be used to quantify the coherence length, l_c values of a light source from the reduction of fringe visibility in the path difference between the two arms [31]. Figure 3 (b) shows a comparison of the measured values for l_c in SM, MM, SW operation schemes. The greatly reduced coherence length can be easily observed for the MM and SW operation schemes. We note that the temporal integration effect in SW operation will also reduce the coherence length. Shown in Fig. 3 (c) is the measured l_c for only a SW VCSEL operation, where this reduction in fringe visibility is emphasized. The calculated l_c = 0.23 mm, is in an

#142244 - $15.00 USD Received 4 Feb 2011; revised 10 May 2011; accepted 16 May 2011; published 18 May 2011

excellent agreement with the measured l_c value of 0.24 mm. These short coherence length values are not as low as the values obtained in an LED (l_c ~9 μm, Δλ~20 nm), but are sufficiently low to greatly reduce temporal noise and spatial statistics of the speckle pattern in SW operation. We hypothesize that the reduction of the coherence length in our studies is similar in origin to previously reported incoherent light emission from pulsed broad-area VCSELS [33]. The spectral width of a VCSEL at a SM operation in Fig. 3 (a) is greatly overestimated due to the limited spectral resolution of the OSA. Applying a Gaussian fit to the measured interferogram values in SM operation yields l_c values over 50 mm. This is somewhat lower than the more traditional single mode laser sources. For example, many laser diodes achieve a linewidth of 100 MHz or lower, and l_c values of the order of meters. The full effects of coherence length on speckle contrast are not completely known. However, as long as the coherence length is much greater than the optical path through tissue, little reduction in contrast is expected. As red light has typical penetration of ~20 mm [17], SM VCSEL operation is well suited for LSCI. Importantly, the change between the high coherence SM and the low coherence SW rapid current sweep operation can be done very rapidly, in a few microseconds, enabling simultaneous portable IOSI and LSCI imaging, using VCSEL light sources, in frame rates over 100 frames/sec. Based on these findings, we focused our analysis on comparing noise values between three cases, namely (i) VCSEL illumination in single mode (SM) operation; (ii) VCSEL illumination in sweep mode (SW) operation; and (iii) LED illumination, demonstrating that by applying the current sweep, coherence effects of a VCSEL can be reduced to produce noise levels similar to those of an LED.

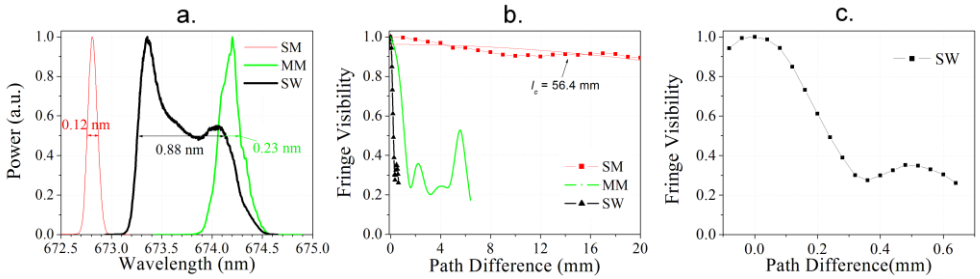

Fig. 3. (a) VCSEL spectral analysis showing narrow single mode (SM), shifted multi-mode (MM) and widened current sweep (SW) spectra. The FWHM spectral width values are indicated inside the figure. b) Measured interferogram envelope for SM VCSEL operation (red), showing characteristically long coherence length. In comparison, the measured envelopes for MM (green) and SW (black) operations are shown. c) Measured interferogram envelope for SW operation, in smaller path difference range. The values of l_c, can be estimated from the fringe visibility vs. path difference values

3.3 Temporal noise and spatial speckle statistics

The quantitative temporal and spatial noise data are summarized in Fig. 4 for stationary opal glass (a), *ex vivo* mouse brain slice (b) and *in vivo* rat brains, for n = 7 rats (c).

The temporal and spatial noise values, shown as standard deviation over mean (σ/μ) intensity values represent spatial and temporal changes of the speckle patterns and can be used to illustrate the benefit of reducing coherence in brain illumination. The error bars represent the standard error. A significant decline in noise values is seen corresponding to decreasing laser coherence. Special care was given to keeping all exposure times and image series length identical between illumination source studies to allow comparison of the noise values. Source placement was also controlled to roughly equalize mean image intensities in all cases, within ~50% to 75% of CCD saturation, mitigating intensity-related shot noise variations.

In stationary opal glass, Fig. 4 (a), there is no inherent movement of the sample. Thus, the spatial noise values are dominant and the comparatively small temporal noise can be

#142244 - $15.00 USD Received 4 Feb 2011; revised 10 May 2011; accepted 16 May 2011; published 18 May 2011

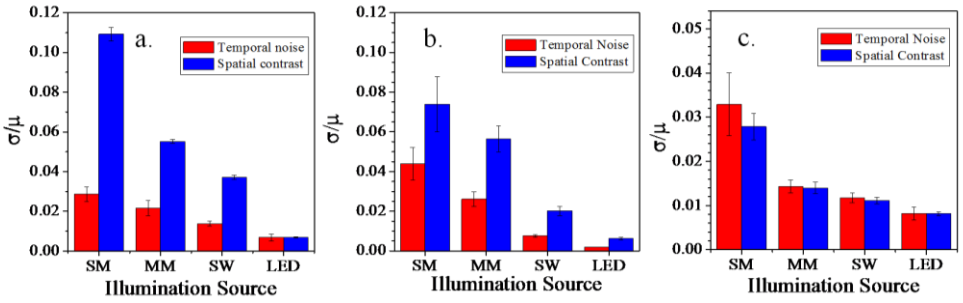

Fig. 4. Standard deviation over mean intensity values that are used to evaluate temporal and spatial noise values. (a) Opal glass, (b) *ex vivo* mouse brain slice, (c) *in vivo* rat brain for n = 7 rats. A significant decline in noise values is seen corresponding to decreasing laser coherence.

presumed to be due to slight vibrations. We note that SM illumination gives the highest noise value, over 10%, while the shorter coherence length of SW illumination corresponds to a reduction in noise by a factor of ~2-3. The stationary surface of opal glass can largely account for this. Speckle values in the light reflected from an opal glass undergo minimal temporal variations and thus the larger CR values in this case correspond to a full range of interference intensities. With LED illumination, both the temporal and spatial noise values are ~0.6% and in excellent agreement with the expected intensity fluctuations due to read noise and shot noise values for the CCD camera we used (*i.e.* for a camera pixel well size of n = 40,000 e-, the estimated shot noise is $\sqrt{n} \approx 200$ e-, representing a 0.5% absolute intensity fluctuations in the image). These values were similarly observed in LED illumination of the brain in agreement with no significant contribution to noise from coherence effects.

In *ex vivo* cortical slices, Fig. 4 (b), we expect spatial as well as temporal variations due to physiological processes in the living tissue. Overall, a similar trend in noise values to the opal glass is observed, with the highest temporal noise values obtained from SM illumination and lower noise values by a factor of ~4-5 in SW illumination. Figure 4 (c) shows the summary of *in vivo* rat brain studies. The increased coherence length in SM illumination results in increased noise values compared with SW and LED illumination, similar to the other cases we have analyzed. Importantly, the total temporal noise in SW illumination is increased (relatively) by 40% as compared to LED illumination, representing a moderate noise increase due to coherence effects in SW illumination, while a much larger increase in noise values (i.e. ~6 fold) is shown in SM VCSEL illumination. Further analysis of noise was conducted by changing the f/# of the optical system between 1.4 and 2.8. The independent contribution of coherent effects to absolute intensity changes and noise values can be estimated by comparing the total noise values to the theoretically predicted noise due to shot noise and the measured read noise values. The absolute intensity changes due to coherence are estimated to be ~0.25-0.5% for this range of f/stop values (as compared to ~0.6% noise values due to shot noise), confirming that the relative contribution of coherence to the total noise is low. Therefore, the SW VCSEL illumination scheme is very effective in reducing these coherence effects in the images resulting in values within 40% of the optimal low noise LED illumination of a live brain. Based on these observed values, we can infer that slight motion on the cranial surface *in vivo* allows us to benefit from some degree of speckle averaging over time. This is further supported by the fact that SM illumination benefits the most *in vivo*, while LED illumination sees virtually no difference between the two situations. In MM operation (shown for comparison in Fig. 4 (a)-(c)), the trend of reduced noise with reduced coherence is preserved.

Alongside the temporal noise values, we plotted the corresponding *in vivo* spatial speckle pattern statistics data (blue), in Fig. 4 (c). The results correlate strongly with the temporal case in all illumination schemes. There is no statistically significant difference between the temporal and spatial noise values in Fig. 4 (c). The similarity between spatial and temporal

#142244 - $15.00 USD Received 4 Feb 2011; revised 10 May 2011; accepted 16 May 2011; published 18 May 2011

values can be associated with slight movements on the cranial surface. In essence, the temporal noise is dominated by coherent elements, varying along with small movements, in lieu of physiologically relevant optical signals. These same varying coherent elements are what we measure in spatial contrast calculations. We can further infer that speckle is indeed the largest source of noise difference between the LED and VCSEL cases. This effect shows up most clearly when we attempt a spatial analysis of a fixed speckle pattern, as shown in Fig. 4 (a). Temporal fluctuations are not dominant and we can discern the powerful effect laser coherence has on noise. In all six cases shown in Fig. 4 (i.e. temporal and spatial noise values in opal glass, *ex vivo* mouse brain slice, and *in vivo* brain) the reduction of the noise values associated with lower illumination source coherence is statistically significant, as can also be shown by the standard error bars plotted in Fig. 4 (a)-(c).

A more qualitative account of the contrast difference between the illumination schemes for *in vivo* rat brain can be obtained from the temporal noise maps given in Fig. 5.

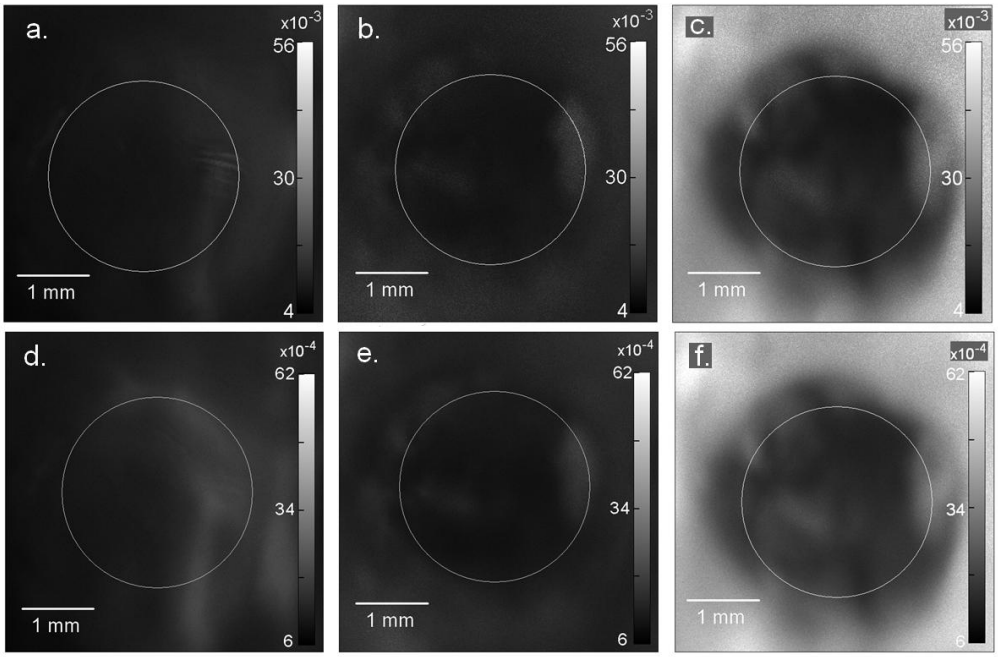

Fig. 5. Temporal noise maps for 3 illumination sources. The pixel-wise standard deviation over mean (σ/μ) intensity values was calculated in each case on 256 frames. (a) LED illumination has low noise throughout. (b) Current sweep (SW) mode illumination has noise levels near that of the LED, particularly on the cortical surface. (c) Single mode (SM) illumination has noise levels an order of magnitude higher than the LED throughout. (d)-(f) show the same analysis repeated, on 256 images binned through 64 trials. While the qualitative characteristics remain similar, we see approximately 1/8 the noise values as seen in the initial case.

The temporal noise maps were calculated from the original images as described in the methods. The marked circle represents the region where the skull is removed and the brain exposed, using a craniotomy. Images in Fig. 5 (a)-(c) show temporal noise maps calculated for a single trial, under LED, SW and SM operations respectively. Average pixel noise values are similar to those found in the previously shown noise analysis. However, due to different locations of the LED and the VCSEL sources with respect to the illuminated brain, these computed noise maps do not look identical. Here, it becomes clear how the coherence effects of the VCSEL manifest. The LED illumination scheme is shown in Fig. 5 (a), in which we see characteristically low noise values, with highlights appearing largely due to high contrast values at dark/light edge features within a frame. As discussed above, the main contribution is

#142244 - $15.00 USD Received 4 Feb 2011; revised 10 May 2011; accepted 16 May 2011; published 18 May 2011

due to shot noise and read noise values for the image. In Fig. 5 (b), SW illumination is shown in a similar intensity scale for comparison. Similar noise values are observed. Qualitatively we can infer that speckle effects can be observed in the image, but not large enough to pass the main contributions from the shot noise. The temporal noise map for SM illumination scheme is shown in Fig. 5 (c) with a much larger intensity scale in and it is evident that laser speckle contributes significantly higher noise values in this case. Although not in best focus, some vascular shadowing on the cortical surface can be seen in a similar manner to images produced from LCSI techniques, as demonstrated below in section 3.4.

Many optical imaging studies in live animals improve the noise performance by trial averaging of the brain imaging study [13,16]. Images in Fig. 5 (d)-(f) show temporal noise maps calculated after a 64 trial averaging under LED, SW and SM operations respectively. The maps are qualitatively very similar to the single trial case. However, we see reduction to a factor of 8 in the corresponding noise values. This is what we would expect as random noise reduction generally scales with the square root of number of trials in a repeated set averaging scheme. The reduction shown here brings noise values in both the LED and SW case to a level low enough to detect small stimulated cortical activity signals, on the order of 10^{-3}-10^{-4} intensity variation.

3.4 Optical neural imaging

In the previous sections we have discussed the reduction of noise in current sweep (SW) operation, and the potential to use this mode to create tissue oxygenation maps. In addition, single mode (SM) operation can be used for imaging blood flow. We show examples for such modalities in this section. Figure 6 shows cortical spreading depression (CSD) propagation in a mouse brain slice, induced by local injection of KCl solution. The brain slice is illuminated with a VCSEL in current sweep (SW) operation and imaged through a low magnification microscope objective (4×). Figure 6 (a), a plot of the average reflected intensity within a cortical ROI for both 10 × 10 and 100 × 100 pixel binning, shows a clear reflectivity change when the spreading depression wave propagates. Figure 6 (b) shows an image of the brain slice. The propagating spreading depression front is clearly visible in this image.

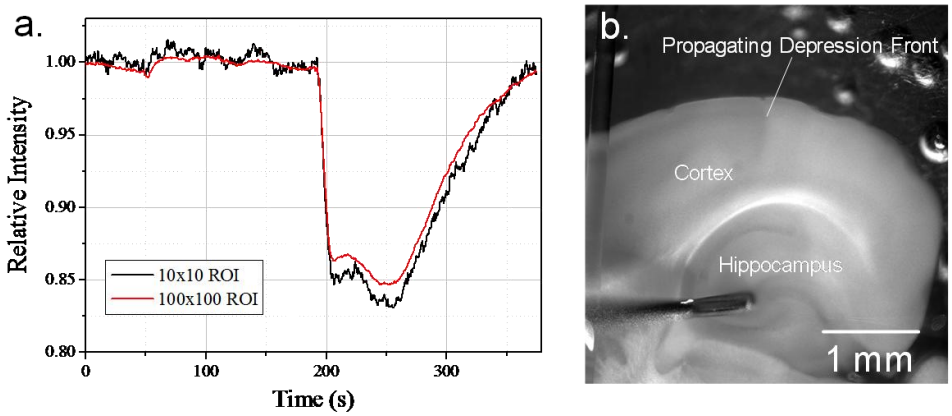

Fig. 6. Cortical spreading depression in a mouse brain slice, illuminated by a VCSEL in current sweep (SW) operation. (a) Average intensity values within a cortical region of interest, a clear reflectivity change is observed during the spreading depression. Two plot lines represent different ROI sizes within the cortex, to show the effects of pixel binning on eliminating excess noise. (b) Brain slice image, during spreading depression propagation.

The changes in blood flow and in tissue reflectance in a live rat brain due to induced ischemia event by closing of the right common carotid artery are shown in Fig. 7. These changes were imaged with the same CCD camera, alternating between SM and SW

#142244 - $15.00 USD Received 4 Feb 2011; revised 10 May 2011; accepted 16 May 2011; published 18 May 2011

illumination schemes respectively, to allow image co-registration. A 500 × 500 pixel ROI was used to allow faster imaging at 14 frames per second (fps), providing both oxygenation and flow images 7 times a second. The current source allows rapid triggering of current waveforms, with output starting within 1 μs of a received trigger, resulting in a triggering scheme solely dependent on the camera frame rate. The slight temporal offset of ~71 ms between imaging modalities, due to alternating frame scheme, can be considered insignificant on the time scale of expected hemodynamic changes, and the two modes can effectively be considered simultaneous.

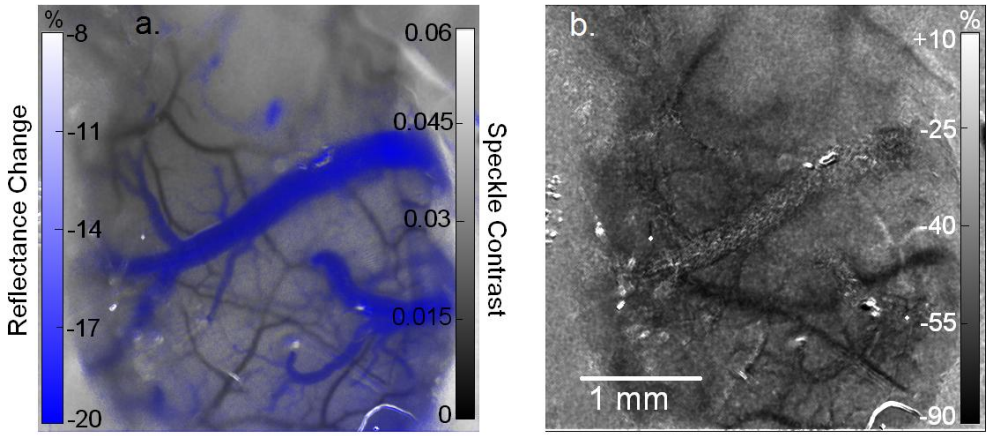

Fig. 7. Imaging of ischemia induced changes in oxygenation and in blood flow in a rat brain. (a) The percent change in reflected intensity (mainly due to deoxy-Hb) during SW operation (blue scale) overlaid on the speckle contrast ratio values measured during SM operation. The blood vessels on the surface of the brain are easily observed, while the overlay with the oxygenation changes illustrates the benefits of a co-registered image. (b) Calculated percent change in flow values. A decrease of the flow values in the blood vessels and capillary bed is observed. Some artifacts can be observed from small bubbles in the cortical window.

Figure 7 (a) shows the calculated percent change in reflected intensity at 670 nm in SW operation when the effect of the ischemia reached its peak, before blood flow in the artery was restored. The data is overlaid above the calculated speckle CR values at that time point using LCSI in SM operation. Regions of higher flow, such as large vessels, have lower CR values and appear darker. A small reduction of the reflected intensity signal (overlaid image, blue) relative to the baseline values can be observed in the whole tissue, while a larger reduction is observed in the vicinity of the blood vessels. At 670 nm, the main contribution to reflected intensity changes is associated with changes in HbR concentration [17]. The observed changes are in good agreement with the expected increase of HbR due to the ischemia condition and reduction of the available oxygen to the tissue [25]. The overlay illustrates the benefits of co-registering the information from the two imaging techniques, using a single camera where the blood vessel topology is emphasized as a background to the localization of induced changes in tissue oxygenation. Figure 7 (b) shows the calculated percent change in blood flow values when the effect of the ischemia reached its peak, as calculated using a simplified LCSI model for long exposure times. The decreased flow values in Fig. 7 (b) are expected, since ischemic induction is expected to produce a reduction in cerebral blood flow (CBF) in the vessels as compared to baseline values. These changes were partially recovered after the tension was removed and blood flow was restored. This data fits well with the expected hemodynamic response in this ischemic animal model. The vessels with the largest reflectance changes are veins, judging by the hemodynamic response and vessel orientations [25]. The map of relative flow can be calculated from the CR maps as shown in Fig. 7 (a) by calculating changes in the correlation time map of the brain. When applying sufficiently long exposure times, $T > \tau_c$, (T ~10 ms), the conversion between CR values to correlation times and relative flow maps can be

#142244 - $15.00 USD Received 4 Feb 2011; revised 10 May 2011; accepted 16 May 2011; published 18 May 2011

greatly simplified [5] as was recently demonstrated in a real time blood flow visualization [4]. Multi-exposure LCSI techniques [6,7,11,34] or dynamic speckle contrast analysis algorithms [35] can assist in accurately quantifying flow rates in vessels obscured by static speckle from the skull, and allow evaluation of the statistical distribution of the blood flow speeds [36], thus improving the sensitivity and accuracy of quantitative flow maps.

4. Discussion

We have evaluated the noise values associated with reflection from a stationary opal glass, *ex vivo* from a mouse brain slice and *in vivo* illuminating a rat brain. The coherence length l_c values for the various VCSEL operating modes were directly measured and were in a good agreement with the observed changes in the VCSEL spectral emission linewidth. There is a good correlation between reduced coherence length to a reduction in the measured spatial and temporal noise values for the various operation schemes we have evaluated. The temporal analysis as portrayed above implies that the reduced coherence noise values (due to a transverse VCSEL mode variations induced by current sweep) allow VCSEL illumination to approach the noise performance of an LED. VCSEL dimensions (~30 μm diameter, 2-20 μm gain profile diameter, 3-10 μm height) are small compared with edge emitting laser diodes [28] and current changes in a VCSEL introduce thermal and polarization changes to the mode spectral and spatial shape that support rapid transverse mode sweep. Due to the latter two characteristics, a VCSEL is more amenable than an edge emitting laser diode to rapid variation of both transverse beam shape and mode characteristics.

Through current sweeping modes, the coherence length of a VCSEL can be reduced to ~0.25 mm. However, it is clear that this is not sufficient to explain the reduction of noise to levels near those of an LED. The LED has a spectral width of nearly 20 nm, an order of magnitude higher that the VCSEL even in sweep current scheme. We assert that mode sweeping only takes us part way to the low noise levels desired. Further reduction is achieved with the assistance of temporal speckle averaging due to slight motion on the cortical surface in living subjects due to breathing, pulsation, and vasomotor movement of brain tissue.

IOSI is one method by which we can apply VCSELs in measuring small reflectance changes associated with neural activity. Through trial averaging, even greater signal-to-noise ratios can be achieved for the measurement of sensory neural activation in rats and mice [16]. Trial averaging results in both LED and VCSEL current sweep mode (SW) reduce temporal noise to a similar level, at which detection of sensory activity is possible. By driving the VCSEL in current sweep mode, we can utilize the VCSEL for imaging as we would use a low noise LED source. Using three such VCSELs (i.e. 670 nm, 797 nm, 850 nm), all fitting within a miniature package, will enable portable spectroscopic analysis in IOSI.

Utilizing this phenomenon, even single laser illumination source under two power schemes can support a dual modality imaging system. Laser wavelength choice can allow monitoring one tissue chromophore, for example HbR. By taking advantage of the strong coherence effects of the VCSEL in single mode, speckle contrast images can be generated to reveal vasculature. The resulting contrast ratio maps as shown in Fig. 7 (a) can be converted to relative flow rate maps. As such, high-brightness VCSELs can act as efficient miniature light sources for simultaneous ISOI and LCSI imaging. We further assert that contrast imaging techniques such as LSCI can be used as a way of isolating landmarks for real-time spatial co-registration. By utilizing the structural landmarks, movement of a sensor with respect to the brain surface can be accounted for, leading to a stable imaging region of interest within which reflectance changes associated with cortical function may be recorded. The speeds achieved with this setup are limited almost entirely by camera frame rate, lending the technique to high speed imaging with a low switch time bottleneck. The current system described can provide both LSCI and IOS images at 7 fps in a 500 × 500 pixel frame size, significantly faster than other recent single camera dual mode systems [25]. Further work will include integrating this setup with faster cameras, to approach speeds of 100 fps, matching

#142244 - $15.00 USD Received 4 Feb 2011; revised 10 May 2011; accepted 16 May 2011; published 18 May 2011

other high speed IOS techniques [22]. Current system resolution of 7.4 μm enables a field of view of 4-8 mm. Further studies currently underway are using higher magnification of 2 × or 4 × , achieving subcellular resolution, with a trade off in SW noise. However, further frame averaging can easily be implemented to reduce this effect and achieve appropriate temporal resolutions.

We see future applications of this approach in live animal studies with chronic portable imaging sensors mounted over the skull over longer time periods. Ongoing studies aim to implement this technique to demonstrate simultaneous portable ISOI and LSCI imaging, using a single VCSEL light source (e.g. at ~670 nm) with rapid alternation of the illumination scheme to minimize or maximize coherence effects. Importantly, such a flexible, highly dynamic illumination technique will allow for straightforward image co-registration between two independent brain imaging modalities. It can also be implemented in portable sensors for monitoring brain activity in freely behaving animals and in the future, for continuous monitoring of brain activity in patients. A further potential application of rapid current sweep in VCSELs is in fluorescence imaging, where speckle reduction allows for uniform high spatial resolution excitation of a marker or dye.

5. Conclusion

We have demonstrated that changing VCSEL operation between single mode and current sweep schemes can be used to manipulate its speckle noise properties, allowing us to use a single light source to image neural tissue via two different modalities: tissue oxygenation (ISOI) and blood flow (LCSI). We show that the current sweep scheme lowers the temporal and spatial noise of the VCSEL to approach values comparable to that of a low noise LED illumination. We attribute this to the combined effect of decreasing the coherence length of the source, and the spatial and polarization superposition of transverse modes that change in space and time (due to current sweep as well as brain movement). The use of VCSEL light sources for optical brain imaging will advance the development of a portable, head-mounted continuous imaging technique for studying the underlying neuronal activity in un-anesthetized animals, and continuous evaluation of brain activity and drug efficacy in clinical settings.

Acknowledgments

The authors are grateful for the helpful discussions and assistance during experiments by Michael Stryker and Cris Niel, Physiology Dept., UC San Francisco and James S. Harris, and Krishna V. Shenoy, Electrical Engineering, Stanford University during the early phases of this project and by Alex Tonkikh, Joe Hayek, and Peter Carlen, Toronto Western Hospital, Toronto. The authors also wish to thank Mary Hibbs-Brenner and Klein Johnson from Vixar, Inc. for assistance in epitaxial growth of VCSEL devices; to Mic Chaudoir from QImaging for helpful discussions and assistance in fast camera operations; and to Xiaofan Jin and Kelvin So for assistance with developing fast computer software for these studies. This work was supported in part through the University of Toronto departmental start-up funds to OL, the Natural Sciences and Engineering Research Council of Canada (NSERC) Discovery Grant RGPIN-355623-08 and by the Networks of Centres of Excellence of Canada, Canadian Institute for Photonic Innovations (CIPI). TDO acknowledges graduate support from a National Defense Science and Engineering Graduate (NDSEG) fellowship, the U.S. Department of Homeland Security, and an SPIE scholarship.

#142244 - $15.00 USD Received 4 Feb 2011; revised 10 May 2011; accepted 16 May 2011; published 18 May 2011